Uncertainties in structural dynamics for composite sandwich panels

C. Chen, Denis Duhamel, Christian Soize

Uncertainties in structural dynamics for composite sandwich panels

C. Chen[(1)], **D. Duhamel**[(2)], **C. Soize**[(1)]

[(1)] University of Marne-la-Vallée, Laboratoire de Mécanique, Institut Navier
5 boulevard Descartes, 77454 Marne-la-Vallée, France

[(2)] Ecole Nationale des Ponts et Chaussées, Laboratoire Analyse Matériaux et Identification, Institut Navier
6-8 avenue Blaise Pascal, 77455 Marne-la-Vallée, France

email: **chaoui.chen@univ-mlv.fr**

Abstract

This paper concerns uncertainties in structural dynamics for composite sandwich panels constituted of two thin carbon-resin skins and one high stiffness closed-cell foam core. Each skin is constituted of two unidirectional plies [60/-60]. Such light composite sandwich panels, manufactured with a same process, generally present a significant dispersion for their Frequency Response Functions (FRF) in the Low-Frequency (LF) and Medium-Frequency (MF) ranges. The objectives of this paper are (1) to study the dispersion due to the process by using experiments (2) to develop a predictive mean mechanical model based on the use of the laminated composite thin plate theory in dynamics and (3) to use a nonparametric probabilistic approach for data and model uncertainties to improve the predictability of the mean model in the MF dynamics.

1. Introduction

It is known that the dynamical responses of the light composite sandwich panels in the medium-frequency range are sensitive to the process used for their manufacturing. In addition, such sandwich panels constitute complex dynamical systems (dynamical behavior of the materials consituting the different layers; interface conditions between two adjacent layers; boundary conditions, etc) and consequently, model uncertainties are induced by the mathematical-mechanical modeling process in which simplifications are introduced. Finally, the parameters of the mathematical-mechanical modeling are not known with a great precision which means that data parameters are uncertain. Consequently, the robustness of the predictive model in the medium-frequency range of such a dynamical system has to be improved.

This paper concerns structural dynamics of composite sandwich panels constituted of two thin carbon-resin skins and one high stiffness closed-cell foam core. Each skin is constituted of 2 unidirectional plies [60/-60]. As written above, it is known that such sandwich panels, manufactured with a same process, generally present a significant dispersion for their Frequency Response Functions (FRF) in the low-requency (LF) range and above all in the medium-frequency (MF) range. The objectives of this paper are (1) to perform an experimental analysis of the frequency-response-functions dispersion due to the process used for manufacturing the sandwich panels, (2) to develop a predictive mean mechanical model based on the use of the laminated composite thin plate theory in dynamics and to compare the numerical simulations with the experiments, and (3) to use a nonparametric probabilistic approach allowing data and model uncertainties to be modeled in order to improve the predictability of the mean model in the LF and MF dynamics.

The nonparametric probabilistic approach used in this paper, has been introduced in Refs. [1,2] and is based on the use of the random matrix theory. In such a probabilistic model, the probability distribution of each random generalized matrix of the dynamical system (generalized mass, damping and stiffness matrices) depends on a dispersion parameter allowing the level of the random fluctuations of each random matrix to be controlled. An experimental estimation of each dispersion parameter for the random generalized mass, damping and stiffness matrices is proposed. The confidence regions of the random frequency response functions are predicted by using the random dynamical system constructed with the nonparametric probabilistic approach of random uncertainties and are compared with the experimental frequency response functions measured for the 8 sandwich panels.

2. Description of the designed panel

The designed panel is a sandwich panel constituted of five layers made of four thin carbon-resin unidirectional plies and one high stiffness closed-cell foam core. This panel is defined with respect to a Cartesian coordinate system $Oxyz$ and is $0.40\,m$ length (Ox axis), $0.30\,m$ width (Oy axis) and $0.01068\,m$ total thickness (Oz axis). The middle plane of the sandwich panel is Oxy et the origine O is located in corner. Each carbon layer is made of a thin carbon-resin ply with a thickness of $0.00017\,m$, a mass density $\rho = 1600\,Kg/m^3$ and whose elasticity constants are: $E_x = 101$ GPa, $E_y = 6.2$ GPa, $\nu_{xy} = 0.32$, $G_{xy} = G_{xz} = G_{yz} = 2.4$ GPa. The first two layers are two carbon-resin unidirectional plies in a [-60/60] layup. The third layer is a closed-cell foam core with a thichness of $0.01\,m$, a mass density of $80\,Kg/m^3$ and elasticity constants: $E_x = E_y = 60$ MPa, $\nu_{xy} = 0$, $G_{xy} = G_{xz} = G_{yz} = 30$ MPa . The fourth and fifth layers are two carbon-resin unidirectional plies in a [60/-60] layup.

3. Manufacturing the sandwich panels

Eight sandwich panels have been manufactured from the designed panel using the same process and the same materials. All the sandwich panels have been baked in the same batch for suppressing the influences of the different baking conditions concerning time and temperature. The different steps for the manufacturing of the sandwich panels are the following. Step 1: cut out the carbon-resine tissue and cut out the foam plate with the dimension of the designed panel. Step 2: for each plate, paste the carbon-resine tissues with the foam plate. Step 3: bake the eight sandwich panels pasted in the previous step in the vacuum oven for solidify the oxygen resin existing in the sandwich. Figure 1 shows step 2 of the manufacturing process for a sandwich panel.

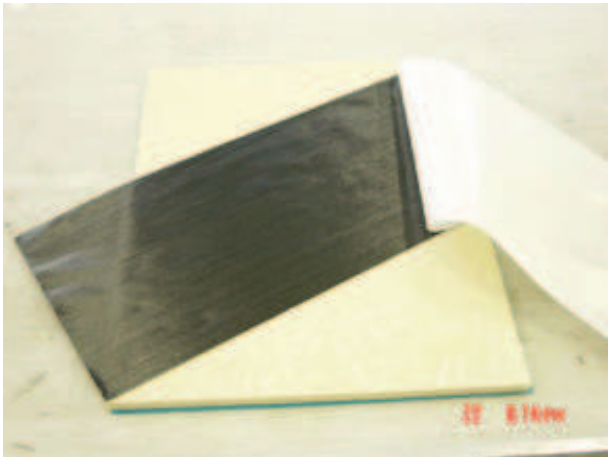

Fig.1: Step 2 of the manufacturing process of a sandwich panel

4. Dynamical identification of the eight sandwich panels

4.1. Description of dynamical testing

The dynamical testing of the eight sandwich panels are realized in the free-free condition. The middle plane of the sandwich panel is vertical and the panel is suspended with a very low eigenfrequency.

The measurements have been performed on the frequency band $[10\,,6000]\,Hz$. Nevertheless, the mean finite element model developed allows only the low- and the medium-frequency bands to be analyzed. Therefore, the frequency band of analysis considered in this paper is the band $B = [10\,,4500]\,Hz$ corresponding to the model validity of the mean finite element model. The input z-force is a point load applied to point $N0$ of coordinates $(0.187, 0.103, 0)\,m$. An electrodynamic shaker delivers a broad band signal. The output z-accelerations are measured at 25 points by accelerometers. For the sake of briefness, the presentation is limited to the 3 following points: $N1$ of coordinates $(0.337, 0.103, 0)\,m$, $N2$ of coordinates $(0.112, 0.159, 0)\,m$ and $N3$ of coordinates $(0.337, 0.216, 0)\,m$. The cross-frequency response functions are identified on frequency band B by using the usual spectral analysis method and signal processing [3,4].

4.2. Experimental cross frequency response functions

Figures 2, 3 and 4 display the graphs of the modulus of the experimental cross frequency response functions in log scale for an input at point $N0$ (driven point) and a transversal acceleration output at points $N1$, $N2$ and $N3$, respectively. There are 8 graphs on each figure corresponding to the 8 sandwich panels. The analysis of the 25 experimental cross frequency response functions on frequency band $B = [10\,,4500]\,Hz$ (in which there are 60 elastic modes) shows a small dispersion in the frequency band $[10\,,1550]\,Hz$ (in which there are 11 elastic modes) and a significant dispersion, increasing with the frequencies, in the frequency band $[1550\,,4500]\,Hz$ (in which there are about 59 elastic modes). This can clearly be seen in figures 2, 3 and 4 relative to points $N1$, $N2$ and $N3$.

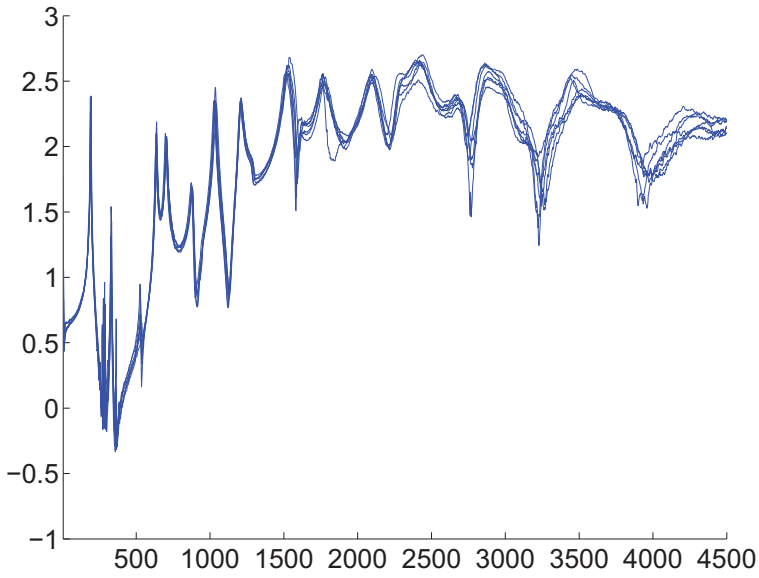

Figure 2: Graphs of the 8 experimental cross FRF between point N0 and point N1 corresponding to the 8 sandwich panels. Horizontal axis: frequency in Hertz. Vertical axis: $\log_{10}$ of the modulus of the acceleration in m/s^2.

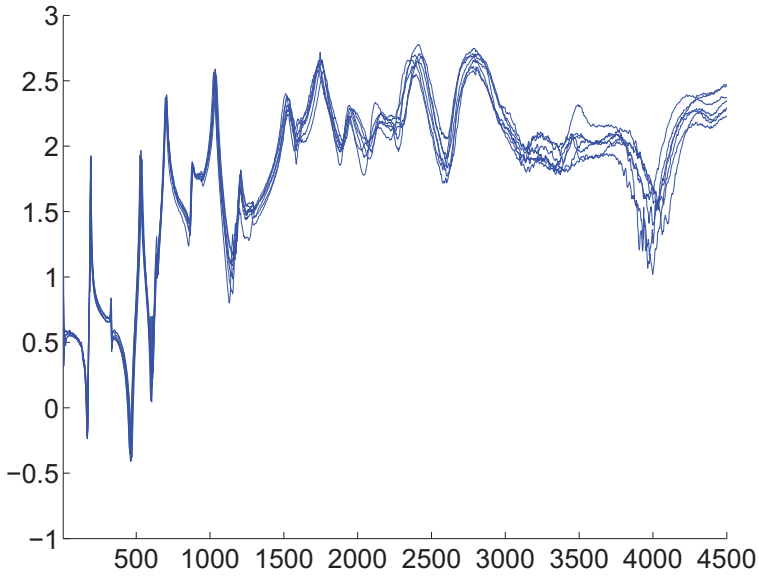

Figure 3: Graphs of the 8 experimental cross FRF between point N0 and point N2 corresponding to the 8 sandwich panels. Horizontal axis: frequency in Hertz. Vertical axis: $\log_{10}$ of the modulus of the acceleration in m/s^2.

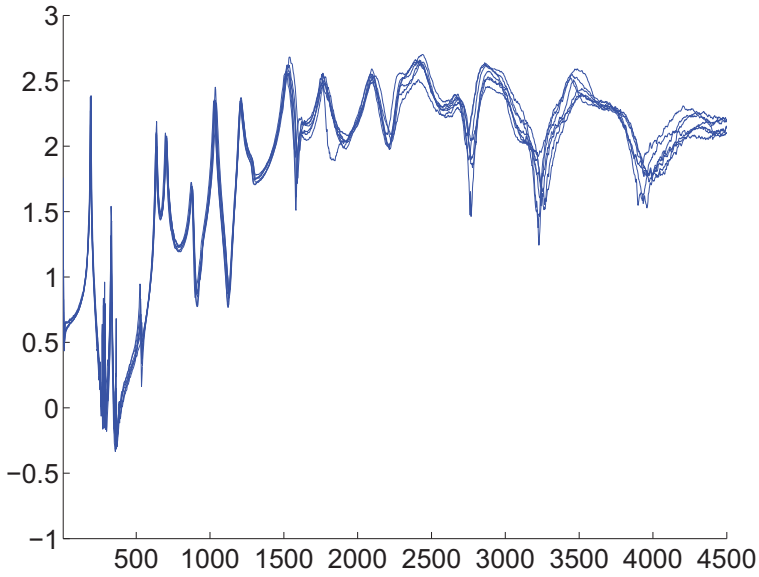

Figure 4: Graphs of the 8 experimental cross FRF between point N0 and point N3 corresponding to the 8 sandwich panels. Horizontal axis: frequency in Hertz. Vertical axis: $\log_{10}$ of the modulus of the acceleration in m/s^2.

4.3. Experimental modal analysis

For each sandwich panel, an experimental modal analysis [5,6] has been performed in the frequency band $[10\,,1550]\,Hz$ using the identified experimental frequency response functions (see Section 4.2). For each sandwich panel $r = 1,\ldots,8$, eleven elastic modes have been identified in this frequency band. For sandwich panel r, the following usual modal parameters of each experimental elastic mode α has been identified: (1) the eigenfrequency $\omega_\alpha^{\exp}(\theta_r)$, (2) the damping rate $\xi_\alpha^{\exp}(\theta_r)$, (3) the elastic mode shape $\psi_\alpha^{\exp}(\theta_r)$ and the corresponding generalized mass $\mu_\alpha^{\exp}(\theta_r)$. Let $\underline{\omega}_\alpha^{\exp} = (1/8)\sum_{r=1}^{8}\omega_\alpha^{\exp}(\theta_r)$ be the average experimental eigenfrequency α. Introducing $\underline{f}_\alpha^{\exp} = \underline{\omega}_\alpha^{\exp}/(2\,\pi)$, the results are

$$\underline{f}_1^{\exp} = 191.0\,Hz \quad , \quad \underline{f}_2^{\exp} = 329.5\,Hz \quad , \quad \underline{f}_3^{\exp} = 532.0\,Hz \quad , \quad \underline{f}_4^{\exp} = 635.1\,Hz \quad .$$

For $\alpha = 1,\ldots,11$, let $\underline{\xi}_\alpha^{\exp} = (1/8)\sum_{r=1}^{8}\xi_\alpha^{\exp}(\theta_r)$ be the average experimental damping rate α and let $\underline{\xi}^{\exp} = (1/11)\sum_{\alpha=1}^{11}\underline{\xi}_\alpha^{\exp}$ be the global average experimental damping rate. The result is

$$\underline{\xi}^{\exp} = 0.01 \quad .$$

5. Mean mechanical model of the dynamical system and experimental comparisons

5.1. Mean finite element model

The designed panel is considered as a laminated composite thin plate for which each layer is made of an orthotropic elastic material in plane stress [7,8,9]. The elasticity constants of each layer are given in Section 2. Since we are interested in the z-dispacement of the middle plane of the sandwich panel in the bending mode and since the panel is a free structure, there are 3 rigid body modes. We are interested in the construction of the responses in the frequency domain over the frequency band of analysis B. The designed panel is modeled by using a regular finite element meshes constituted of 64×64 four-nodes finite elements for laminated plate bending. The damping of the structure is introduced by an arbitrary usual model controlled by the modal damping rates (see section 5.2) In frequency band B, the mean finite element model of linear vibrations of the free designed panel around a position of static equilibrium taken as reference configuration without prestresses is written as

$$\left(-\omega^2\,[\,\underline{\mathbb{M}}\,] + i\omega\,[\,\underline{\mathbb{D}}\,] + [\,\underline{\mathbb{K}}\,]\right)\,\underline{\mathbf{y}}(\omega) = \underline{\mathbf{f}}(\omega) \quad , \quad \omega\in B \quad , \tag{1}$$

in which $\underline{\mathbf{y}}(\omega) = (\underline{y}_1(\omega),\ldots,\underline{y}_m(\omega))$ is the $\mathbb{C}^m$-vector of the m DOFs (displacements and rotations) and $\underline{\mathbf{f}}(\omega) = (\underline{f}_1(\omega),\ldots,\underline{f}_m(\omega))$ is the $\mathbb{C}^m$-vector of the m inputs (forces and moments). The mean mass matrix $[\,\underline{\mathbb{M}}\,]$ is a

positive-definite symmetric $(m \times m)$ real matrix. The mean damping and stiffness matrices $[\underline{\mathbb{D}}]$ and $[\underline{\mathbb{K}}]$ are positive-semidefinite symmetric $(m \times m)$ real matrices (free structure). Matrices $[\underline{\mathbb{D}}]$ and $[\underline{\mathbb{K}}]$ have the same null space having a dimension $m_{\text{rig}} = 3$ and spanned by the rigid body modes $\{\underline{\boldsymbol{\varphi}}_{-2}, \underline{\boldsymbol{\varphi}}_{-1}, \underline{\boldsymbol{\varphi}}_0\}$. It is assumed that the given deterministic load vector $\underline{\mathbf{f}}(\omega)$ is in equilibrium, i.e. is such that $< \underline{\mathbf{f}}(\omega) , \underline{\boldsymbol{\varphi}}_{1-\beta} >= 0$ for all β in $\{1, 2, 3\}$, in which, for all $\mathbf{u}$ and $\mathbf{v}$ in $\mathbb{C}^m$, $< \mathbf{u} , \mathbf{v} >= u_1 \, v_1 + \ldots + u_m \, v_m$. For all ω in B, Eq. (1) has a unique solution $\underline{\mathbf{y}}(\omega) = [\underline{\mathbb{T}}(\omega)] \, \underline{\mathbf{f}}(\omega)$ in which $[\underline{\mathbb{T}}(\omega)]$ is the matrix-valued FRF (frequency response function) defined by $[\underline{\mathbb{T}}(\omega)] = [\underline{\mathbb{A}}(\omega)]^{-1}$ where $[\underline{\mathbb{A}}(\omega)]$ is the dynamic stiffness matrix such that

$$[\underline{\mathbb{A}}(\omega)] = -\omega^2 \, [\underline{\mathbb{M}}] + i\omega \, [\underline{\mathbb{D}}] + [\underline{\mathbb{K}}] \quad . \tag{2}$$

5.2. Mean reduced matrix model

The mean reduced matrix model adapted to frequency band B is constructed by using the usual modal analysis with the elastic modes of the associated conservative system. The generalized eigenvalue problem associated with the mean mass and stiffness matrices of the mean finite element model is written as $[\underline{\mathbb{K}}] \, \underline{\boldsymbol{\varphi}} = \underline{\lambda} \, [\underline{\mathbb{M}}] \, \underline{\boldsymbol{\varphi}}$. Since $[\underline{\mathbb{K}}]$ is a positive-semidefinite matrix, we have $\underline{\lambda}_{-2} = \underline{\lambda}_{-1} = \underline{\lambda}_0 = 0 < \underline{\lambda}_1 \leq \underline{\lambda}_2 \leq \ldots \leq \underline{\lambda}_m$ and the associated elastic modes $\{\underline{\boldsymbol{\varphi}}_1, \underline{\boldsymbol{\varphi}}_2, \ldots\}$ corresponding to the strictly positive eigenvalues $\underline{\lambda}_1, \underline{\lambda}_2, \ldots$, are such that $< [\underline{\mathbb{M}}] \, \underline{\boldsymbol{\varphi}}_\beta , \underline{\boldsymbol{\varphi}}_{\beta'} >= \underline{\mu}_\beta \, \delta_{\beta\beta'}$ and $< [\underline{\mathbb{K}}] \, \underline{\boldsymbol{\varphi}}_\beta , \underline{\boldsymbol{\varphi}}_{\beta'} >= \underline{\mu}_\beta \, \underline{\omega}_\beta^2 \, \delta_{\beta\beta'}$ in which $\underline{\omega}_\beta = \sqrt{\underline{\lambda}_\beta}$ is the eigenfrequency of elastic mode $\underline{\boldsymbol{\varphi}}_\beta$ whose normalization is defined by the generalized mass $\underline{\mu}_\beta$. The mean reduced matrix model of the dynamic system whose mean finite element model is defined by Eq. (1) is obtained by constructing the projection of the mean finite element model on the subspace V_n of $\mathbb{R}^m$ spanned by $\{\underline{\boldsymbol{\varphi}}_1, \ldots, \underline{\boldsymbol{\varphi}}_n\}$ with $n \ll m$. Let $[\underline{\Phi}_n]$ be the $(m \times n)$ real matrix whose columns are vectors $\{\underline{\boldsymbol{\varphi}}_1, \ldots, \underline{\boldsymbol{\varphi}}_n\}$. The generalized force $\mathbf{F}^n(\omega)$ is an $\mathbb{C}^n$-vector such that $\mathbf{F}^n(\omega) = [\underline{\Phi}_n]^T \, \mathbf{f}(\omega)$. The generalized mass, damping and stiffness matrices $[\underline{M}_n]$, $[\underline{D}_n]$ and $[\underline{K}_n]$ are positive-definite symmetric $(n \times n)$ real matrices such that $[\underline{M}_n]_{\beta\beta'} = \underline{\mu}_\beta \, \delta_{\beta\beta'}$, $[\underline{D}_n]_{\beta\beta'} =< [\underline{\mathbb{D}}] \, \underline{\boldsymbol{\varphi}}_{\beta'} , \underline{\boldsymbol{\varphi}}_\beta >$ and $[\underline{K}_n]_{\beta\beta'} = \underline{\mu}_\beta \, \underline{\omega}_\beta^2 \, \delta_{\beta\beta'}$. In general, $[\underline{D}_n]$ is a full matrix. Nevertheless, as explained in section 5.1, the damping model is introduced in writing that $[\underline{D}_n]_{\beta\beta'} = 2 \, \underline{\xi}_\beta \, \underline{\mu}_\beta \, \underline{\omega}_\beta \, \delta_{\beta\beta'}$ in which $\underline{\xi}_1, \ldots, \underline{\xi}_n$ are the mean modal damping rates. The mean damping model is then chosen (see Section 4.3) such that

$$\underline{\xi}_1 = \ldots = \underline{\xi}_n = \underline{\xi}^{\text{exp}} = 0.01 \quad .$$

For frequency band B, the mean reduced matrix model of the dynamic system is written as the approximation $\underline{\mathbf{y}}^n(\omega)$ of $\underline{\mathbf{y}}(\omega)$ such that

$$\underline{\mathbf{y}}^n(\omega) = [\underline{\Phi}_n] \, \underline{\mathbf{q}}^n(\omega) \quad , \quad \omega \in B \quad , \tag{3}$$

in which the $\mathbb{C}^n$-vector $\underline{\mathbf{q}}^n(\omega)$ of the generalized coordinates is the unique solution of the mean reduced matrix equation,

$$\left(-\omega^2 \, [\underline{M}_n] + i\omega \, [\underline{D}_n] + [\underline{K}_n] \right) \, \underline{\mathbf{q}}^n(\omega) = \underline{\mathbf{F}}^n(\omega) \quad , \quad \omega \in B \quad , \tag{4}$$

with $\underline{\mathbf{F}}^n(\omega) = [\underline{\Phi}_n]^T \, \underline{\mathbf{f}}(\omega) \in \mathbb{C}^n$ and where the mean generalized mass, damping and stiffness matrices are the positive-definite symmetric $(n \times n)$ real diagonal matrices defined above.

5.3. Updating the conservative part of the mean model with the first experimental eigeinfrequencies

The calculation of the first eigenfrequencies of the designed panel has been performed with the mean finite element model (see Section 5.1) whose finite element mesh is made of 128×64 four-nodes finite elements and for which all the mechanical parameters are defined in Section 2, in particular, for which, for each carbon-resine ply,

$$\rho = 1600 \, Kg/m^3 \quad , \quad E_x = 101 \, GPa \quad , \quad E_y = 6.2 \, GPa \quad ,$$

For the designed panel, the first four computed eigenfrequencies are

$$\underline{f}_1 = 176.4 \, Hz \quad , \quad \underline{f}_2 = 344.8 \, Hz \quad , \quad \underline{f}_3 = 499.7 \, Hz \quad , \quad \underline{f}_4 = 651.2 \, Hz \quad .$$

The mass and the stiffness matrices of the mean finite element model have been updated in order to minimize the cost function

$$J(\rho, E_x, E_y) = \sum_{\beta=1}^{4} |\underline{f}_\beta - \underline{f}_\beta^{\text{exp}}| \quad ,$$

with respect to mass density ρ and to Young moduli E_x and E_y of each carbon-resin ply, where

$$\underline{f}_1^{\text{exp}} = 191.0\,Hz \quad , \quad \underline{f}_2^{\text{exp}} = 329.5\,Hz \quad , \quad \underline{f}_3^{\text{exp}} = 532.0\,Hz \quad , \quad \underline{f}_4^{\text{exp}} = 635.1\,Hz \quad ,$$

are the average experimental eigenfrequencies defined in Section 4.3, and where all the other mechanical parameters (except for ρ, E_x, E_y) take the values defined in Section 2. The updated values are:

$$\rho^{\text{upd}} = 1904\,Kg/m^3 \quad , \quad E_x^{\text{upd}} = 103\,GPa \quad , \quad E_y^{\text{upd}} = 6.0\,GPa \quad ,$$

and yields for the first four updated eigenfrequencies,

$$\underline{f}_1^{\text{upd}} = 191.7\,Hz \quad , \quad \underline{f}_2^{\text{upd}} = 332.8\,Hz \quad , \quad \underline{f}_3^{\text{upd}} = 529.5\,Hz \quad , \quad \underline{f}_4^{\text{upd}} = 630.8\,Hz \quad .$$

Below, the updated mechanical parameters are used instead of the values defined for the designed panel. The designed panel with the updated mechanical constants will be named the updated designed panel associated with the updated mean finite element model and the updated mean reduced matrix model.

5.4. Convergence with respect to the mesh size for the updated designed panel

A convergence of the cross frequency response functions of the updated designed panel has been performed with respect to the size mesh of the finite element mesh. Figure 5 displays the graphs of the cross FRF between point $N0$ and point $N1$ for the three finite element meshes: 32×32 four-nodes finite elements, 64×64 four-nodes finite elements and 128×64 four-nodes finite elements. All the results obtained, and in particular Figure 5, show that the convergence with respect to the finite element mesh size is reasonable for 64×64 four-nodes finite elements.

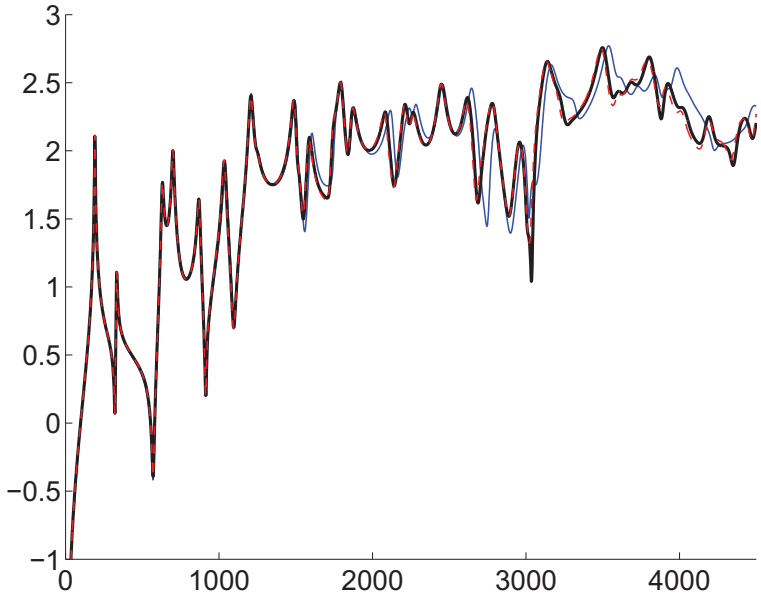

Figure 5: Convergence of the cross frequency response function between point $N0$ and point $N1$ for three finite element meshes: 32×32 (thin solid line), 64×64 (thick solid line), 128×64 (thin dashed line). Horizontal axis: frequency in Hertz. Vertical axis: $\log_{10}$ of the modulus of the acceleration in m/s^2.

5.5. Convergence of the updated mean reduced matrix model with respect to the number of elastic modes

The convergence with respect to the dimension of the updated mean reduced matrix model is analyzed in studing the graph of the L^2-norm in space (over all the middle plane of the sandwich panel) and in frequency (over all the frequency band of analysis B) of the z-acceleration response for a unit input applied to point $N0$. Figure 6 displays the graph of this norm versus the dimension of the updated mean reduced matrix model, that is to say, versus the number of elastic modes. Tha convergence is reached for $n = 120$.

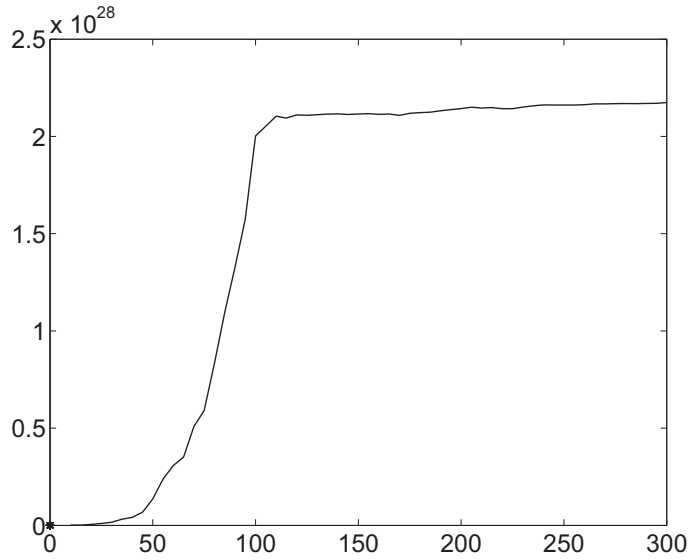

Figure 6: Convergence of the L^2-norm in space and in frequency of z-acceleration response (vertical axis) versus the dimension of the updated mean reduced matrix model (horizontal axis).

5.6. FRF calculation with the updated mean reduced matrix model and experimental comparisons

The cross frequency response functions are calculated by using Eqs. (3) and (4) (updated mean reduced matrix model) with $n = 200$. Figures 7, 8 and 9 display the graphs of the modulus of the experimental and numerical cross frequency response functions in log scale for an input at point $N0$ (driven point) and a z-acceleration output at points $N1$,$N2$ and $N3$, respectively. There are 9 graphs on each figure: 8 graphs correspond to the experimental cross-frequency response functions associated with the 8 sandwich panels and 1 graph corresponds to the numerical cross-frequency response function computed with the updated mean reduced matrix model.
The comparisons of the experimental cross frequency response functions with those constructed with the updated mean finite element model are reasonably good in the frequency band $[0,\ 1500]\,Hz$ and are relatively bad in $[1500\,,4500]\,Hz$. In the frequency band $[1500,\ 4500]\,Hz$, the lack of predictability is increasing with the frequency and is mainly due to data uncertainties (mechanical parameters) and to model uncertainties (modeling the sandwich panel by using the laminated composite thin plate theory).

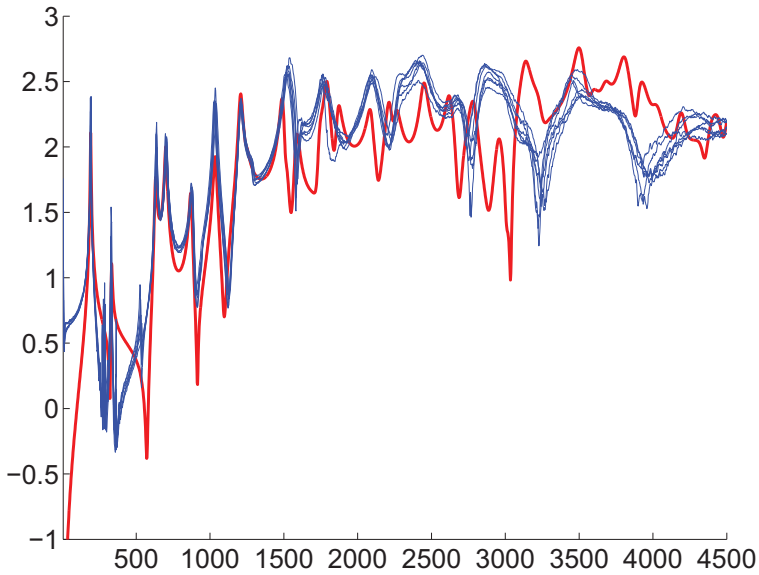

Figure 7: Graphs of the cross FRF between point $N0$ and point $N1$. Horizontal axis: frequency in Hertz. Vertical axis: $\log_{10}$ of the modulus of the acceleration in m/s^2. Experimental cross FRF corresponding to the 8 panels (8 thin solid lines). Numerical cross FRF calulated with the updated mean reduced matrix model (thick solid line)

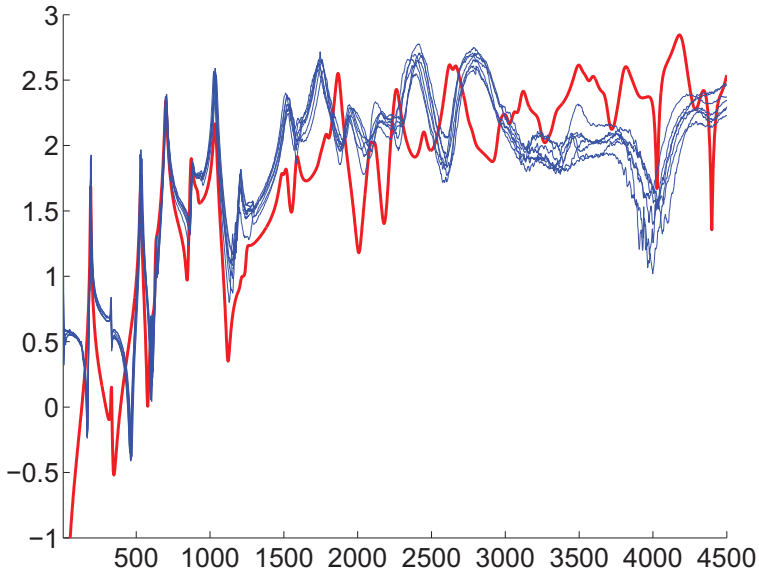

Figure 8: Graphs of the cross FRF between point $N0$ and point $N2$. Horizontal axis: frequency in Hertz. Vertical axis: $\log_{10}$ of the modulus of the acceleration in m/s^2. Experimental cross FRF corresponding to the 8 panels (8 thin solid lines). Numerical cross FRF calulated with the updated mean reduced matrix model (thick solid line)

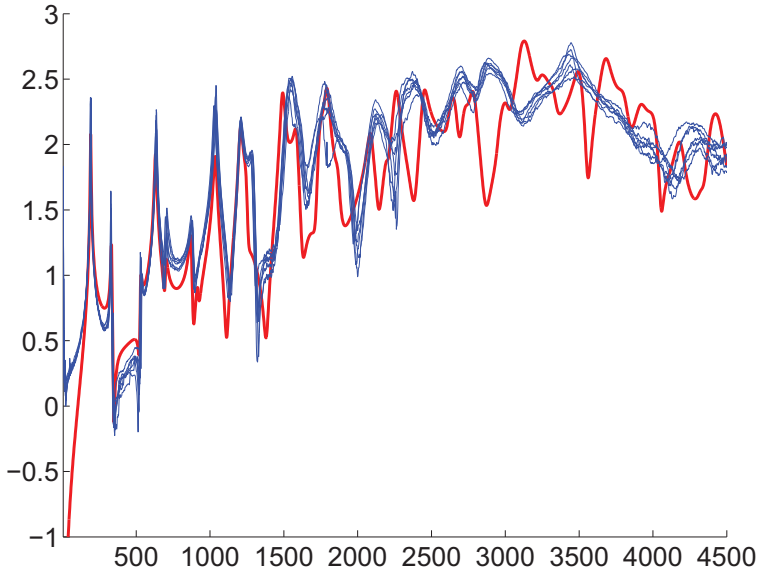

Figure 9: Graphs of the cross FRF between point $N0$ and point $N3$. Horizontal axis: frequency in Hertz. Vertical axis: $\log_{10}$ of the modulus of the acceleration in m/s^2. Experimental cross FRF corresponding to the 8 panels (8 thin solid lines). Numerical cross FRF calulated with the updated mean reduced matrix model (thick solid line)

6. Nonparametric Model of Random Uncertainties

The nonparametric model of random uncertainties has been introduced in Ref. [1]. The construction of the nonparametric model of random uncertainties in the frequency band B consists in modeling the generalized mass, damping and stiffness matrices of the mean reduced matrix model defined by Eqs. (3) and (4) by random matrices $[\mathbf{M}_n]$, $[\mathbf{D}_n]$ and $[\mathbf{K}_n]$. Consequently, the nonparametric model of random uncertainties in frequency band B is written as

$$\mathbf{Y}^n(\omega) = [\underline{\Phi}_n]\, \mathbf{Q}^n(\omega) \quad , \tag{5}$$

in which, for all ω fixed in B, the $\mathbb{C}^n$-valued random variable $\mathbf{Q}^n(\omega)$ of the random generalized coordinates is the unique solution of the random reduced matrix equation,

$$\left(-\omega^2\,[\mathbf{M}_n] + i\omega\,[\mathbf{D}_n] + [\mathbf{K}_n]\right)\, \mathbf{Q}^n(\omega) = \underline{\mathbf{F}}^n(\omega) \quad , \quad \omega \in B \quad . \tag{6}$$

From Refs. [1,2], these random matrices are written as

$$[\mathbf{M}_n] = [\underline{L}_{M_n}]^T\,[\mathbf{G}_{M_n}]\,[\underline{L}_{M_n}] \quad , \tag{7}$$

$$[\mathbf{D}_n] = [\underline{L}_{D_n}]^T\,[\mathbf{G}_{D_n}]\,[\underline{L}_{D_n}] \quad , \tag{8}$$

$$[\mathbf{K}_n] = [\underline{L}_{K_n}]^T\,[\mathbf{G}_{K_n}]\,[\underline{L}_{K_n}] \quad , \tag{9}$$

in which the positive-definite $(n \times n)$ real diagonal matrices $[\underline{L}_{M_n}]$, $[\underline{L}_{D_n}]$ and $[\underline{L}_{K_n}]$ are such that $[\underline{M}_n] = [\underline{L}_{M_n}]^2$, $[\underline{D}_n] = [\underline{L}_{D_n}]^2$ and $[\underline{K}_n] = [\underline{L}_{K_n}]^2$. The full random matrices $[\mathbf{G}_{M_n}]$, $[\mathbf{G}_{D_n}]$ or $[\mathbf{G}_{K_n}]$ are mutually independent and the dispersion of random matrices $[\mathbf{G}_{M_n}]$, $[\mathbf{G}_{D_n}]$ and $[\mathbf{G}_{K_n}]$ are controlled by the positive real parameters δ_M, δ_D and δ_K which are independent of dimension n and do not depend on frequency ω. If A_n denotes M_n, D_n or K_n, then the dispersion parameter δ_A of random matrix $[\mathbf{A}_n]$ is defined by

$$\delta_A = \left\{ \frac{1}{n} \| \, [\mathbf{G}_{A_n}] - [I_n] \, \|_F^2 \right\}^{1/2} \quad , \tag{10}$$

in which $\|[\,H\,]\|_F$ is the Frobenius norm of real matrix $[\,H\,]$ such that $\|[\,H\,]\|_F^2 = \mathrm{tr}\{[\,H\,]^T[\,H\,]\}$ and then, the random matrix $[\mathbf{G}_{A_n}]$, with dispersion parameter δ_A, is defined by

$$[\mathbf{G}_{A_n}] = [\mathbf{L}_{A_n}]^T\,[\mathbf{L}_{A_n}] \quad , \tag{11}$$

in which $[\mathbf{L}_{A_n}]$ is an upper triangular random $(n \times n)$ real matrix such that the random variables $\{[\mathbf{L}_{A_n}]_{jj'}, j \leq j'\}$ are mutually independent and such that

(1) for $j < j'$, real-valued random variable $[\mathbf{L}_{A_n}]_{jj'}$ is written as $[\mathbf{L}_{A_n}]_{jj'} = \sigma_n U_{jj'}$ in which $\sigma_n = \delta_A (n+1)^{-1/2}$ and where $U_{jj'}$ is a real-valued Gaussian random variable with zero mean and variance equal to 1;

(2) for $j = j'$, positive-valued random variable $[\mathbf{L}_{A_n}]_{jj}$ is written as $[\mathbf{L}_{A_n}]_{jj} = \sigma_n \sqrt{2 V_j}$ in which σ_n is defined above and where V_j is a positive-valued gamma random variable whose probability density function $p_{V_j}(v)$ with respect to dv is written as $p_{V_j}(v) = \mathbb{1}_{\mathbb{R}^+}(v) \{\Gamma(\frac{n+1}{2\delta_A^2} + \frac{1-j}{2})\}^{-1}\; v^{\frac{n+1}{2\delta_A^2} - \frac{1+j}{2}}\; e^{-v}$.

7. Experimental estimation of the dispersion parameters for the nonparametric probabilistic model

Let δ_M, δ_D and δ_K be the dispersion parameters of the random generalized mass, damping and stiffness matrices. Since the dispersion parameters have to be independent of n (see Section 6), the dispersion parameters can be estimated by using the experimental matrices $[\,M_\nu^{\exp}(\theta_r)]$, $[\,D_\nu^{\exp}(\theta_r)]$ and $[\,K_\nu^{\exp}(\theta_r)]$ for $r = 1, \ldots, 8$ corresponding to the 8 experimental sandwich panels, and for a dimension $\nu < n$. Here, a very simple procedure is proposed for estimating δ_M, δ_D and δ_K (this procedure corresponds to the first step of the procedure based on the maximum likelihood principle and developed in Ref. [10]. The first step of this procedure consists in associating the ν first elastic modes computed with the updated mean finite element model, with the corresponding ν experimental elastic modes obtained by performing the experimental modal analysis [5,6] of each sanswich panel. Let $0 < \omega_{j_1}^{\exp}(\theta_r) \leq \ldots \leq \omega_{j_\nu}^{\exp}(\theta_r)$ be the set of the ν experimental eigenfrequencies of sandwich panel r, corresponding to the set of the ν first eigenfrequencies $0 < \underline{\omega}_1 \leq \ldots \leq \underline{\omega}_\nu$ computed with the updated mean finite element model. The same set of degrees of freedom for the mean finite element model and for the experimental sandwich panels is considered (25 observations).

For each sandwich panel $r = 1, \ldots, 8$, the association of the first experimental elastic modes ordered with increasing eigenfrequencies (which means that $j_1 = 1, \ldots, j_\nu = \nu$), with the first elastic modes computed with the updated mean finite element model and ordered with increasing eigenfrequencies, has been performed using the $[\mathrm{MAC}(\theta_r)]$ matrix defined by

$$[\mathrm{MAC}(\theta_r)]_{\alpha\beta} = \frac{< \underline{\boldsymbol{\varphi}}_\beta \, , \boldsymbol{\psi}_\alpha^{\exp}(\theta_r) >^2}{< \underline{\boldsymbol{\varphi}}_\beta \, , \underline{\boldsymbol{\varphi}}_\beta > < \boldsymbol{\psi}_\alpha^{\exp}(\theta_r) \, , \boldsymbol{\psi}_\alpha^{\exp}(\theta_r) >} \quad ,$$

in which $\underline{\boldsymbol{\varphi}}_\beta$ is the elastic mode of the updated mean finite element model whose eigenfrequency is $\underline{\omega}_\beta$ and where $\boldsymbol{\psi}_\alpha^{\exp}(\theta_r)$ is the experimental elastic mode of sandwich panel r whose eigenfrequeny is $\omega_\alpha^{\exp}(\theta_r)$. Figure 10 displays the graph $(\alpha, \beta) \mapsto [\mathrm{MAC}(\theta_r)]_{\alpha\beta}$ for a given r. A similar figure is obtained for any other sandwich panel. Figure 10 shows that the diagonal terms are dominant which means that there is a good correlation between any experimental elastic mode and the numerical elastic mode having the same order.

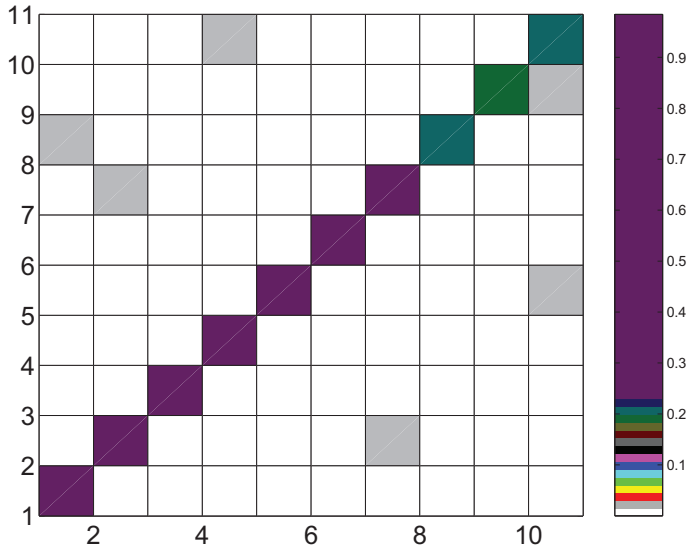

Figure 10: Graph of $(\alpha, \beta) \mapsto [\mathrm{MAC}(\theta_r)]_{\alpha\beta}$. Horizontal axis: α (rank of the experimental elastic modes). Vertical axis: β (rank of the elastic modes computed with the updated mean reduced matrix model). Dark diagonal terms: MAC between 0.77 and 0.98. Grey extradiagonal terms: MAC between 0.06 and 0.1. White extradiagonal terms: MAC less than 0.03.

Thus, for a given set of m degrees of freedom, let $[\Psi_\nu^{\exp}(\theta_r)]$ be the $(m \times \nu)$ real matrix whose columns are the ν elastic modes of experimental sandwich panel r associated with the first experimental eigenfrequencies $0 < \omega_1^{\exp}(\theta_r) \leq \ldots \leq \omega_\nu^{\exp}(\theta_r)$ and let $[\underline{\Phi}_\nu]$ be the $(m \times \nu)$ real matrix whose columns are the ν first elastic modes calculated with the updated mean finite element model and associated with eigenfrequencies $0 < \underline{\omega}_1 \leq \ldots \leq \underline{\omega}_\nu$. Let $[\widetilde{M}_\nu^{\exp}(\theta_r)]$, $[\widetilde{D}_\nu^{\exp}(\theta_r)]$ and $[\widetilde{K}_\nu^{\exp}(\theta_r)]$ be the corresponding experimental generalized mass, damping and stiffness matrices of experimental sandwich panel r directly deduced from the experimental modal analysis and such that $[\widetilde{M}_\nu^{\exp}(\theta_r)]_{\alpha\alpha'} = \mu_\alpha^{\exp}(\theta_r)\delta_{\alpha\alpha'}$, $[\widetilde{D}_\nu^{\exp}(\theta_r)]_{\alpha\alpha'} = 2\xi_\alpha^{\exp}(\theta_r)\mu_\alpha^{\exp}(\theta_r)\omega_\alpha^{\exp}(\theta_r)\delta_{\alpha\alpha'}$ and $[\widetilde{K}_\nu^{\exp}(\theta_r)]_{\alpha\alpha'} = \mu_\alpha^{\exp}(\theta_r)\,(\omega_\alpha^{\exp}(\theta_r))^2\delta_{\alpha\alpha'}$. Let $[\mathbf{M}_\nu]$, $[\mathbf{D}_\nu]$ and $[\mathbf{K}_\nu]$ be the random matrices associated with the mean reduced matrix model of dimension ν and defined in Section 6. Since the experimental elastic modes differ from the elastic modes constructed with the updated mean finite element model (due to uncertainties), matrices $[\widetilde{M}_\nu^{\exp}(\theta_r)]$, $[\widetilde{D}_\nu^{\exp}(\theta_r)]$ and $[\widetilde{K}_\nu^{\exp}(\theta_r)]$ are not represented in the same vector subspace than $[\mathbf{M}_\nu]$, $[\mathbf{D}_\nu]$ and $[\mathbf{K}_\nu]$ (or equivalently than $[\underline{M}_\nu]$, $[\underline{D}_\nu]$ and $[\underline{K}_\nu]$). However, it can be written that

$$[\Psi_\nu^{\exp}(\theta_r)]\,\widetilde{\mathbf{q}}^{\exp}(\theta_r) = [\underline{\Phi}_\nu]\,\mathbf{q}^{\exp}(\theta_r) \quad , \tag{12}$$

in which $\widetilde{\mathbf{q}}^{\exp}(\theta_r)$ is the $\mathbb{C}^m$-vector of the experimental generalized coordinates and where $\mathbf{q}^{\exp}(\theta_r)$ is the corresponding $\mathbb{C}^m$-vector of the generalized coordinates in the mean-model basis. By construction, the matrix $[\Psi_\nu^{\exp}(\theta_r)]^T\,[\Psi_\nu^{\exp}(\theta_r)] \in \mathbb{M}_\nu(\mathbb{R})$ is invertible. Introducing the left pseudo-inverse $\left([\Psi_\nu^{\exp}(\theta_r)]^T\,[\Psi_\nu^{\exp}(\theta_r)]\right)^{-1}$ $[\Psi_\nu^{\exp}(\theta_r)]^T \in \mathbb{M}_{\nu,m}(\mathbb{R})$ of $[\Psi_\nu^{\exp}(\theta_r)] \in \mathbb{M}_{m,\nu}(\mathbb{R})$, Eq. (12) yields

$$\widetilde{\mathbf{q}}^{\exp}(\theta_r) = [S_\nu^{\exp}(\theta_r)]\,\mathbf{q}^{\exp}(\theta_r) \quad , \tag{13}$$

in which the matrix $[S_\nu^{\exp}(\theta_r)] \in \mathbb{M}_\nu(\mathbb{R})$ is written as

$$[S_\nu^{\exp}(\theta_r)] = \left([\Psi_\nu^{\exp}(\theta_r)]^T\,[\Psi_\nu^{\exp}(\theta_r)]\right)^{-1}[\Psi_\nu^{\exp}(\theta_r)]^T\,[\underline{\Phi}_\nu] \quad . \tag{14}$$

The matrix transformation defined by Eqs. (13)-(14) allows the experimental matrices $[\widetilde{M}_\nu^{\exp}(\theta_r)]$, $[\widetilde{D}_\nu^{\exp}(\theta_r)]$ and $[\widetilde{K}_\nu^{\exp}(\theta_r)]$ to be transformed into the matrices $[M_\nu^{\exp}(\theta_r)]$, $[D_\nu^{\exp}(\theta_r)]$ and $[K_\nu^{\exp}(\theta_r)]$, which are defined by

$$\begin{aligned}
[M_\nu^{\exp}(\theta_r)] &= [S_\nu^{\exp}(\theta_r)]^T\,[\widetilde{M}_\nu^{\exp}(\theta_r)]\,[S_\nu^{\exp}(\theta_r)] \in \mathbb{M}_\nu^+(\mathbb{R}) \\
[D_\nu^{\exp}(\theta_r)] &= [S_\nu^{\exp}(\theta_r)]^T\,[\widetilde{D}_\nu^{\exp}(\theta_r)]\,[S_\nu^{\exp}(\theta_r)] \in \mathbb{M}_\nu^+(\mathbb{R}) \\
[K_\nu^{\exp}(\theta_r)] &= [S_\nu^{\exp}(\theta_r)]^T\,[\widetilde{K}_\nu^{\exp}(\theta_r)]\,[S_\nu^{\exp}(\theta_r)] \in \mathbb{M}_\nu^+(\mathbb{R}) \quad .
\end{aligned} \tag{15}$$

Noting A as M, D or K, we can then introduce the matrix $[G_\nu^{\exp}(\theta_r)] \in \mathbb{M}_n^+(\mathbb{R})$ such that $[A_\nu^{\exp}(\theta_r)] = [\underline{L}_{A_\nu}]^T [G_\nu^{\exp}(\theta_r)] [\underline{L}_{A_\nu}]$ in which the invertible upper triangular matrix $[\underline{L}_{A_\nu}] \in \mathbb{M}_\nu(\mathbb{R})$ is such that $[\underline{A}_\nu] = [\underline{L}_{A_\nu}]^T [\underline{L}_{A_\nu}] \in \mathbb{M}_n^+(\mathbb{R})$. Therefore, matrix $[G_\nu^{\exp}(\theta_r)]$ is given by the equation,

$$[G_\nu^{\exp}(\theta_r)] = [\underline{L}_{A_\nu}]^{-T} [A_\nu^{\exp}(\theta_r)] [\underline{L}_{A_\nu}]^{-1} \in \mathbb{M}_\nu^+(\mathbb{R}) \quad . \tag{16}$$

Consequently, 8 realizations $\{[G_\nu^{\exp}(\theta_r)], r = 1, \ldots, 8\}$ of random matrix $[\mathbf{G}_\nu]$ defined by Eq. (11) have effectively been constructed. The dispersion parameter δ_A of random matrix $[\mathbf{A}_n]$ being defined by Eq. (10), for a fixed value of ν, we introduce the parameter $\delta_A(\nu)$, depending on ν, such that

$$\delta_A(\nu) = \left\{ \frac{1}{8\nu} \sum_{r=1}^{8} \| [G_\nu^{\exp}(\theta_r)] - [I_\nu] \|_F^2 \right\}^{1/2} \quad . \tag{17}$$

Since $\delta_A(\nu)$ is an increasing function of ν for large values of ν due to the inscreasing of random uncertainties with the frequencies, the dispersion parameter δ_A of random matrix $[\mathbf{A}_n]$ is then defined by

$$\delta_A = \min_{\nu \geq 2} \delta_A(\nu) \quad . \tag{18}$$

Figure 11 displays the graphs of functions $\nu \mapsto \delta_M(\nu)$, $\nu \mapsto \delta_D(\nu)$ and $\nu \mapsto \delta_K(\nu)$. It can be seen that the minima are obtained for $\nu = 5$ and consequently, Eq. (18) yields $\delta_M = 0.23$, $\delta_D = 0.43$ and $\delta_K = 0.25$ for random matrices $[\mathbf{M}_n]$, $[\mathbf{D}_n]$ and $[\mathbf{K}_n]$ (these values are independent of dimension n of the random reduced matrix model).

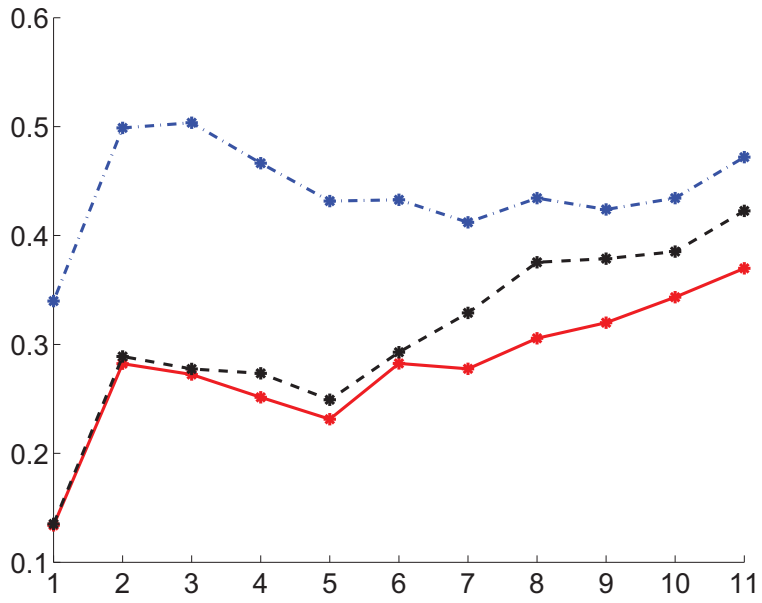

Figure 11: Graphs of functions $\nu \mapsto \delta_M(\nu)$(solid line), $\nu \mapsto \delta_D(\nu)$ (dashdot line) and $\nu \mapsto \delta_K(\nu)$ (dashed line). Horizontal axis: ν. Vertical axis: δ.

8. Confidence region prediction for the FRF and experimental comparisons

8.1. Confidence region prediction with the nonparametric probabilistic model

We are interested in the construction of the confidence region associated with a probability level $P_c = 0.98$ for the modulus of the random cross frequency response functions between point $N0$ and points $N1$, $N2$ and $N3$. Let $\omega \mapsto W(\omega) = | - \omega^2 \mathbf{Y}_k^n(\omega)|$ in which k is the degree of freedom corresponding to the z-displacement at point $N1$, $N2$ and $N3$, and where $\mathbf{Y}^n(\omega)$ is the random vector given by Eqs. (5) and (6). This confidence region is constructed by using the quantiles. For ω fixed in B, let $F_{W(\omega)}$ be the cumulative distribution function (continuous from the right) of random variable $W(\omega)$ which is such that $F_{W(\omega)}(w) = P(W(\omega) \leq w)$. For $0 < p < 1$, the pth quantile or fractile of $F_{W(\omega)}$ is defined as

$$\zeta(p) = \inf\{w : F_{W(\omega)}(w) \geq p\} \quad . \tag{19}$$

Then, the upper envelope $w^+(\omega)$ and the lower envelope $w^-(\omega)$ of the confidence region are defined by

$$w^+(\omega) = \zeta(1-P_c) \quad , \quad w^-(\omega) = \zeta(P_c) \quad . \tag{20}$$

The estimation of $w^+(\omega)$ and $w^-(\omega)$ is performed by using the sample quantiles [11]. Let $w_1(\omega) = W(\omega;\theta_1), \ldots, w_{n_s}(\omega) = W(\omega;\theta_{n_s})$ be the n_s independent realizations of random variable $W(\omega)$ associated with the independent realizations $\theta_1, \ldots, \theta_{n_s}$. Let $\widetilde{w}_1(\omega) < \ldots < \widetilde{w}_{n_s}(\omega)$ be the order statistics associated with $w_1(\omega), \ldots, w_{n_s}(\omega)$. Therefore, one has the following estimation

$$w^+(\omega) \simeq \widetilde{w}_{j^+}(\omega) \quad , \quad j^+ = \text{fix}(n_s(1-P_c)) \quad , \tag{21}$$

$$w^-(\omega) \simeq \widetilde{w}_{j^-}(\omega) \quad , \quad j^- = \text{fix}(n_s P_c) \quad , \tag{22}$$

in which $\text{fix}(z)$ is the integer part of the real number z.

The confidence region of the random cross frequency response functions are calculated by using Eqs. (5)-(11) and (21)-(22). Random Eqs. (5) and (6) are solved by using the Monte Carlo numerical simulation with n_s realizations. The realization $\mathbf{Q}^n(\omega;a_\ell)$ of the $\mathbb{C}^n$-valued random variable $\mathbf{Q}^n(\omega)$ is the solution of the deterministic matrix equation

$$\left(-\omega^2\,[\mathbf{M}_n(a_\ell)] + i\omega\,[\mathbf{D}_n(a_\ell)] + [\mathbf{K}_n(a_\ell)]\right)\,\mathbf{Q}^n(\omega;a_\ell) = \underline{\mathbf{F}}^n(\omega) \quad , \quad \omega \in B \quad . \tag{23}$$

in which $[\mathbf{M}_n(a_\ell)]$, $[\mathbf{D}_n(a_\ell)]$ and $[\mathbf{K}_n(a_\ell)]$ are the realizations of the random matrices $[\mathbf{M}_n]$, $[\mathbf{D}_n]$ and $[\mathbf{K}_n]$ respectively. The convergence of the random solution of Eq. (6) with respect to the number n_s of realizations can be analyzed in studying the mapping

$$n_s \mapsto \text{conv}(n_s) = \frac{1}{n_s}\sum_{\ell=1}^{n_s}\int_B \|\mathbf{Q}^n(\omega;a_\ell)\|^2\,d\omega \quad , \tag{24}$$

in which $\mathbf{Q}^n(\omega;a_1), \ldots, \mathbf{Q}^n(\omega;a_{n_s})$ are the n_s realizations of the $\mathbb{C}^n$-valued random variable $\mathbf{Q}^n(\omega)$. Figure 12 displays the graph of the function $n_s \mapsto \text{conv}(n_s)$ for $n = 200$. The convergence is reached for $n_s = 1200$.

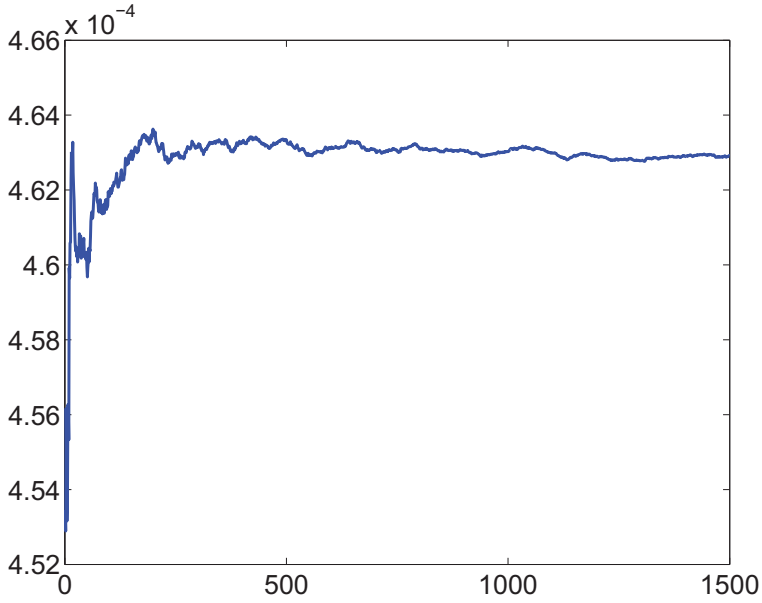

Figure 12: Convergence of the random solution with respect to the number of realizations: Graph of function $n_s \mapsto \text{conv}(n_s)$. Horizontal axis: n_s. Vertical axis: $\text{conv}(n_s)$.

8.2. Prediction and experimental comparison

Figures 12, 13 and 14 display the confidence region prediction for the random cross frequency response functions between point $N0$ and points $N1$, $N2$ and $N3$ respectively, calculated with $n_s = 2000$ realizations and $n = 200$. These figures show how the experimental cross FRF corresponding to the 8 panels are positioned with respect to this confidence region. In addition, each figure displays the graph of the numerical cross FRF calculated with the

updated mean reduced matrix model and the graph of the mean value of the random cross FRF calculated with the nonparametric probabilistic model.

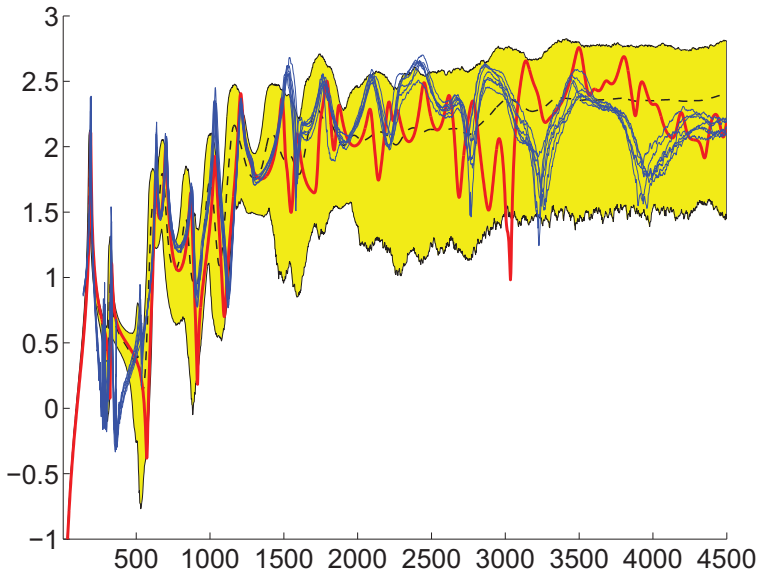

Figure 12: Confidence region prediction for the random cross FRF between point $N0$ and point $N1$. Horizontal axis: frequency in Hertz. Vertical axis: $\log_{10}$ of the modulus of the acceleration in m/s^2. Experimental cross FRF corresponding to the 8 panels (8 thin solid lines). Numerical cross FRF calculated with the updated mean reduced matrix model (thick solid line). Mean value of the random cross FRF calculated with the nonparametric probabilistic model (thin dashed line). Confidence region of the random cross FRF calculated with the nonparametric probabilistic model (grey region).

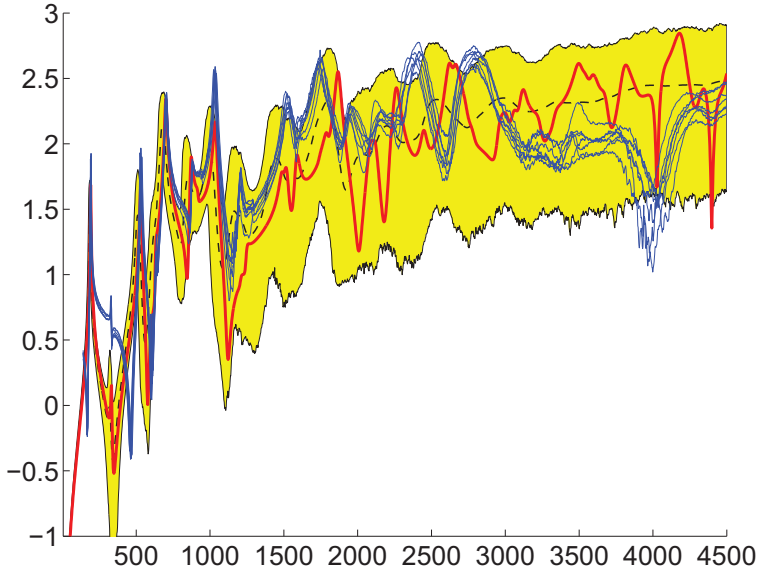

Figure 13: Confidence region prediction for the random cross FRF between point $N0$ and point $N2$. Horizontal axis: frequency in Hertz. Vertical axis: $\log_{10}$ of the modulus of the acceleration in m/s^2. Experimental cross FRF corresponding to the 8 panels (8 thin solid lines). Numerical cross FRF calculated with the updated mean reduced matrix model (thick solid line). Mean value of the random cross FRF calculated with the nonparametric probabilistic model (thin dashed line). Confidence region of the random cross FRF calculated with the nonparametric probabilistic model (grey region).

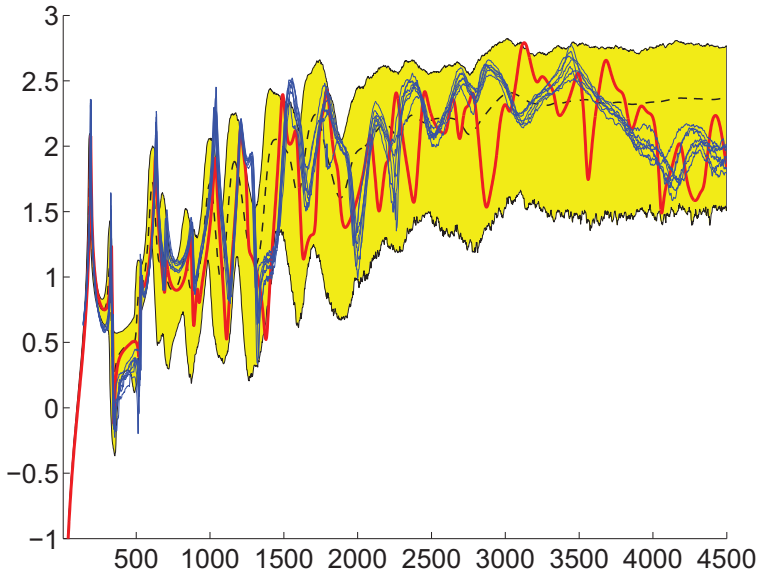

Figure 14: Confidence region prediction for the random cross FRF between point $N0$ and point $N3$. Horizontal axis: frequency in Hertz. Vertical axis: $\log_{10}$ of the modulus of the acceleration in m/s^2. Experimental cross FRF corresponding to the 8 panels (8 thin solid lines). Numerical cross FRF calculated with the updated mean reduced matrix model (thick solid line). Mean value of the random cross FRF calculated with the nonparametric probabilistic model (thin dashed line). Confidence region of the random cross FRF calculated with the nonparametric probabilistic model (grey region).

9. Conclusions

The experimental results obtained for a set of 8 light sandwich panels show the sensitivity of the dynamical response of the panels in the medium-frequency range. Such sandwich panels have to be considered as complex dynamical systems in the medium-frequency range. The use of the simplified usual laminated composite thin plate theory, for constructing the predictive dynamical mean model, introduces significant model uncertainties. Since such dynamical systems are very sensitive to uncertainties and taking into account the presence of data and model uncertainties in the mean mechanical model, the introduction of a probabilistic model of random uncertainties is necessary to improve the predictability of the mean model. A nonparametric probabilistic approach for modeling random uncertainties is used. A methodology is proposed to indentify the dispersion parameters of the probability model of the generalized mass, damping and stiffness full random matrices. The confidence regions of the cross frequency response functions of the stochastic systems are then constructed and are compar(ed to the experimental cross frequency response functions for the 8 sandwich panels. The prediction compared with the experiments is good enough.

References

[1] C. Soize, *A Nonparametric Model of Random Uncertainties on Reduced Matrix Model in Structural Dynamics*, Probabilistic Engineering Mechanics, Vol. 15, No. 3 (2000), pp. 277-294.

[2] C. Soize, *Maximum entropy approach for modeling random uncertainties in transient elastodynamics*, J. Acoust. Soc. Amer., Vol. 109, No. 5 (2001),pp. 1979-1996.

[3] K. McConnell, *Vibration Testing. Theory and Practice*, Wiley Interscience, New York (1995).

[4] J. S. Bendat, A. G. Piersol, *Engineering Applications of Correlation and Spectral Analysis*, John Wiley And Sons, New York, 1980.

[5] D. Ewins, *Modal Testing: Theory and Practice*, John Wiley and Sons, Inc., New York (1984).

[6] E. Balmes, *Structural Dynamics Toolbox for Use with Matlab*, Sceintific Software (2000).

[7] O.O. Ochoa, J.N. Reddy, *Finite Element Analysis of Composite Laminates*, Kluwer Academic Publishers (1992).

[8] J.N. Reddy, *Mechanics of Laminated Composite Plates*, CRC Press (1997).

[9] R.M. Jones, *Mechanics of Composite Materials*, Taylor and Francis (1999).

[10] C. Soize, Random matrix theory for modeling uncertainties in computational mechanics, *Computer Methods in Applied Mechanics and Engineering* (accepted for publication in March 2004)

[11] R.J. Serfling, *Approximation Theorems of Mathematical Statistics*, John Wiley & Sons (1980).